Received 4 April 2023; accepted 20 April 2023. Date of publication 27 April 2023; date of current version 9 May 2023.

Digital Object Identifier 10.1109/OJAP.2023.3270939

Circularly-Polarized Patch Antennas With Enhanced Bandwidth Based on Capacitively Coupled Orthogonal Patch Radiators

QIONG-SEN WU [1], XIAO-YU TANG [2], XIAO ZHANG [3] (Member, IEEE), LEI ZHU [4] (Fellow, IEEE), GARY ZHANG [1,5], AND CHUN-BING GUO [1]

[1]School of Integrated Circuits, Guangdong University of Technology, Guangzhou 510006, China

[2]School of Information Engineering, Guangdong University of Technology, Guangzhou 510006, China

[3]Guangdong Provincial Mobile Terminal Microwave and Millimeter-Wave Antenna Engineering Research Center, College of Electronics and Information Engineering, Shenzhen University, Shenzhen 518060, China

[4]Department of Electrical and Computer Engineering, Faculty of Science and Technology, University of Macau, Macau, SAR, China

[5]Synergy Innovation Institute of GDUT, Heyuan 517000, China

CORRESPONDING AUTHOR: X. ZHANG (e-mail: xiao.zhang@szu.edu.cn)

This work was supported in part by the National Natural Science Foundation of China under Grant 62001124; in part by the Natural Science Foundation of Guangdong Province under Grant 2022A1515011504; in part by the Science and Technology Projects in Guangzhou under Grant 202201010324; and in part by the Shenzhen Science and Technology Innovation Commission through Shenzhen Fundamental Research Program under Grant JCYJ20190808115411853.

ABSTRACT Circularly-polarized (CP) patch antennas with enhanced bandwidth based on capacitively coupled orthogonal patch radiators are proposed. Several patch radiators are alternately arranged one by one along the *x*- and *y*-direction, producing orthogonal currents and far fields. The adjacent patch radiators are coupled to each other and the coupling structure not only contributes to power distribution but also introduces 90° phase shift for circularly-polarized radiation. There is no need for an additional feeding circuit in the design. The far-field components are mapped to the excitation voltage of the equivalent circuit model and a quantitative design method based on the equivalent circuit model is proposed. The theoretical axial ratio response can be predicted and analyzed. Wideband CP patch antennas with 3 and 4 coupled radiators under a profile of $0.035\lambda_0$ are designed, fabricated, and measured as examples. Full-wave simulation results agree well with the theoretical ones. Multiple minima in the axial ratio response are produced to form wide bandwidth. The measured overlap bandwidths of reflection coefficient, realized gain, and axial ratio for these two antennas are 4.9% and 6.3%, respectively.

INDEX TERMS Wide bandwidth, circular polarization, quantitative design, coupled radiator.

I. INTRODUCTION

CIRCULARLY polarized patch antennas are utilized in many wireless communication systems, such as satellite communications, unmanned aerial vehicles, wireless sensors, global navigation satellite systems (GNSS), and worldwide interoperability for microwave access (WiMAX). Many different types of CP antennas have been developed [1], [2], [3] and CP patch antennas are widely utilized because of low profile and ease of integration with other models. One of the fundamental drawbacks of CP patch antennas is the narrow bandwidth, particularly the axial ratio (AR) bandwidth, which is caused by the resonance characteristic. Numerous efforts have been undertaken in recent years to overcome this problem.

Many wideband CP patch antennas have been reported so far. One class of these antennas is based on the modified radiators. Patch antennas with corner cuts or modified slots are proposed [4], [5], [6], however the bandwidth improvement is only modest. Lower patch radiator quality factors can result from increasing patch height. In order to increase the bandwidth of a conventional CP patch antenna, thick substrate and capacitive probe correction have been used [7], [8].

Wideband CP patch antennas have been designed by including stacked patches [9], [10], parasitic elements [11], [12], [13], [14], pins [15], or metasurfaces [16] as well. Two more orthogonal modes are introduced by the stacked or gap-coupled patch to broaden the bandwidth [17]. Parasitic elements or metasurfaces are introduced to rearranged the current distribution of the antenna and achieve the equal magnitude and 90° phase difference of two orthogonal far fields in a wide band. However, the coupling between the main patch and stacked patches or parasitic elements is often complicated in practice. Furthermore, it is difficult to calculate radiations from the parasitic elements or metasurfaces. As a result, there is currently no synthesis method available for the precise and effective design of these CP antennas. Despite the fact that the characteristic mode method can be used to extract the mode behavior of CP antennas [18], [19], [20], full-wave simulation for parameter sweep and optimization is still required.

Another class of wideband CP patch antennas is based on external feeding circuits. In [21], the impact of amplitude and phase imbalance on a dual differential fed patch antenna is analyzed. Beamwidth is increased by optimizing the phase imbalance of feeding circuits. A coupler [22] or a combination of Wilkinson power divider and quarter-wavelength delay line [23] is also commonly used in traditional feeding circuits. Since the resistor of coupler and Wilkinson power divider absorbs the unbalanced power, two ways of signals with the required phase and magnitude can be achieved in a wide band. Unfortunately, due to the power consumption of the resistor, this kind of CP patch antennas suffers from low radiation efficiency and low power capacity. The bandwidth of CP patch antennas can be further expanded by using the power divider cascaded with a wideband 90° phase shifter [24], [25], [26], [27], [28]. Feeding circuits with metamaterial-line are also utilized to design wideband CP patch antennas [29], [30]. However, because these feeding circuits occupy a large non-radiating area, the entire antenna structure becomes more complicated and expensive. Linearly-polarized filtering antennas have been proposed in recent years. The feeding circuit and the patch antenna are considered as a whole bandpass filter network, where the patch antenna is modeled as the last resonator and the output port [31], [32]. This method has been developed to design wideband CP patch antennas. The bandpass feeding circuit is designed to provide equal excitation of two orthogonal modes of a patch antenna and then CP radiation is obtained by separating two orthogonal modes [33] or inserting a 90° phase delay line [34], [35]. Later in [36], both the magnitude and phase responses are considered in the circuit model in order to achieve multiple AR minima and enhanced bandwidth in a co-design procedure. Furthermore, bandpass filtering circuits with modified resonators [37], [38], [39] are also demonstrated for wideband CP patch antennas. However, the feeding circuits of these antennas still occupy large area and the parasitic radiation from the resonators could degrade the CP performance.

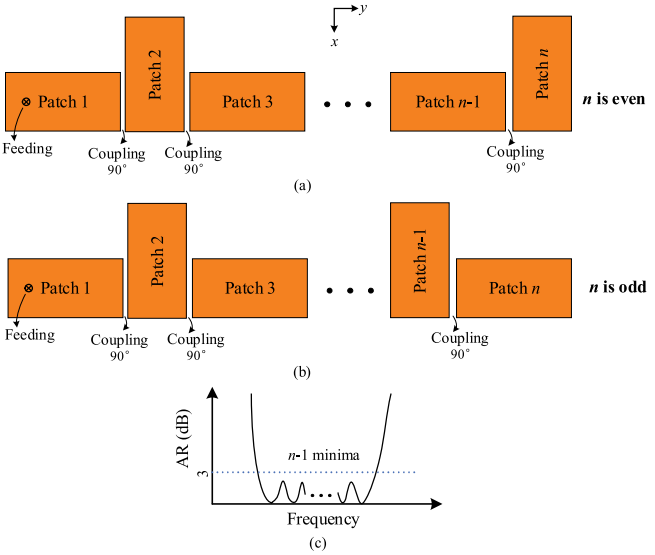

FIGURE 1. The geometry of the proposed CP antenna with n capacitively coupled orthogonal patch radiators. (a) n is even. (b) n is odd. (c) Theoretical AR response. The infinite ground and substrate are not shown.

In this paper, capacitively coupled orthogonal patch radiators are employed to design CP patch antennas with enhanced bandwidth. As shown in Fig. 1, n coupled patch radiators are placed one by one along the x- and y-axes, with one patch radiator adjacent to another one. A coupled-resonator filter network is formed by cascaded orthogonal patches, with the coupling between each two adjacent patches determining the power division and phase shift. In theory, $n - 1$ AR minima come up to achieve enhanced AR bandwidth, as shown in Fig. 1(c). The wide bandwidth of the proposed antenna is achieved by the multiple resonances of the multiple capacitively coupled orthogonal patch antennas. If n coupled patch antennas are employed, n orthogonal modes come up. $n - 1$ AR minima can be achieved by each two neighboring modes. At the frequencies of AR minima, the coupling coefficients of coupled patches are calculated to satisfy the requirement of equal magnitude and 90° phase difference of orthogonal far fields. As a result, the wide bandwidth of the proposed antenna is achieved. In contrast to the conventional CP antenna with parasitic patches, the coupling effect between patches is clearly characterized and the response is accurately predicted with the circuit model in this work. Different from the reported filtering CP patch antennas, the proposed antennas in this work require no external feeding circuits and the patches themselves serve as radiators and feeding networks simultaneously.

II. CP ANTENNA WITH THREE COUPLED RADIATORS

A. GEOMETRY

Fig. 2 shows the proposed CP antenna with 3 coupled patch radiators, which is implemented on a single-layer substrate. Three patch radiators are placed one by one along the x- and y-axes and the patch radiator is in proximity to another one. To minimize the effect of higher-order modes and ensure

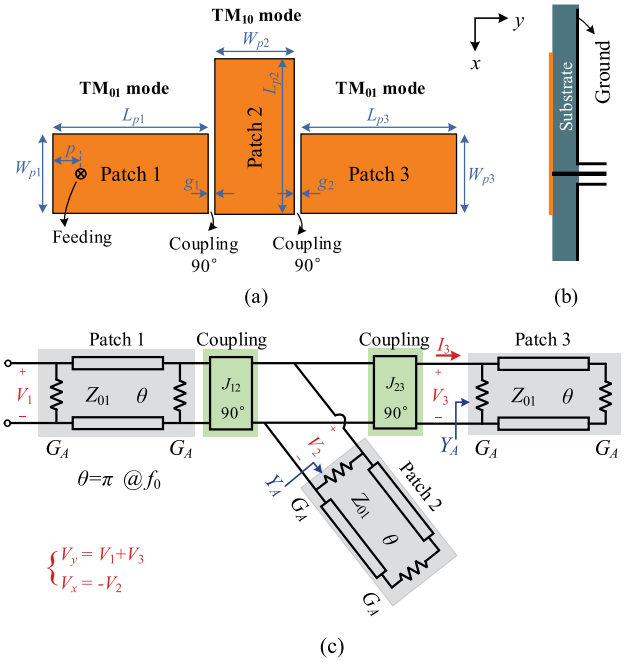

FIGURE 2. The geometry and equivalent circuit model of the proposed CP antenna with 3 coupled radiators. (a) Top view. (b) Side view. (c) Equivalent circuit model.

adequate coupling between patch radiators, the width of the patch radiator is smaller than its the length. TM_{01} modes are excited in Patch 1 and 3, while TM_{10} mode is excited in Patch 2. Thus, the radiations of Patch 1 and 3 are dominated by the x-direction surface currents and the radiation of Patch 2 is dominated by the y-direction surface currents. The couplings between patch radiators transmit power and introduce 90° phase shift at the same time. As a result, two orthogonal far-field components with equal magnitude and 90° phase difference will be produced for CP radiation. A coaxial probe is then placed along the center line of Patch 1 for excitation and impedance matching.

B. EQUIVALENT CIRCUIT MODEL AND QUANTITATIVE DESIGN

Next, as shown in Fig. 2(c), the proposed CP antenna with three radiator elements is efficiently designed based on the equivalent circuit model. To simplify the analysis, the dimensions of the three patch radiators are set to be identical and the resonant frequency of the patch is f_0. As well known, the patch antenna can be equivalent as a half-wavelength transmission line with two parallel radiation conductances at two ends. The characteristic impedance and electrical length of the transmission line are represented by Z_{01} and θ, respectively, and the radiation conductance is denoted as G_A. The couplings between Patch 1 and 2 and between Patch 2 and 3 are modeled as the J inverters with characteristic admittances of J_{12} and J_{23}, respectively. The J inverter has a phase shift of 90°.

It should be noted that the patch radiator is usually equivalent to the parallel resonator with the lumped capacitor, inductor, and conductance in the design of traditional CP patch antennas. However, the phase shift of transmission cannot be accounted for with this lumped element circuit model. For example, the phase shift of the lumped parallel resonator is 0° at the resonant frequency. But actually, when the signal passes through a single patch, there is a 180° phase shift. Therefore, the transmission-line model is more accurate for the patch radiator in this design.

In the design of the conventional CP patch antennas, as discussed in [23], [40], [41], the voltages (V_x and V_y) of the patch resonators in the equivalent circuit model correspond to the radiation fields. As a result, the magnitude ratio and phase difference of two orthogonal far-field components in this design can be expressed as $|V_y/V_x|$ and $\varphi(V_y/V_x)$, respectively. Referring to the geometry and equivalent circuit model in Fig. 2, the complex amplitude ratio of the two orthogonal components is given by

$$\frac{V_y}{V_x} = \frac{V_1 + V_3}{-V_2} = \frac{V_1/V_3 + 1}{-V_2/V_3} \tag{1}$$

where V_1, V_2, and V_3 stand for the excitation voltages of Patches 1, 2, and 3, respectively. Next, V_1 and V_2 are tried to be expressed by V_3.

$$Y_A = \frac{I_3}{V_3} = G_A + Y_{01}\frac{G_A + jY_{01}\tan\theta}{Y_{01} + jG_A\tan\theta} \tag{2}$$

where $Y_{01} = 1/Z_{01}$.

The patch can be considered as a half-wavelength resonator and its susceptance slope is $b_r = \pi Y_{01}/2$. According to the definitions of the quality factor and J inverter, the quality factor of the patch and the coupling coefficients between the adjacent patch radiators are given by

$$Q = \frac{b_r}{2G_A} = \frac{\pi}{4}\frac{Y_{01}}{G_A} \tag{3}$$

$$k_{12} = \frac{J_{12}}{b_r} = \frac{2J_{12}}{\pi Y_{01}} \quad k_{23} = \frac{J_{23}}{b_r} = \frac{2J_{23}}{\pi Y_{01}} \tag{4}$$

where Q is the quality factor of the single patch radiator. J_{12} is the characteristic admittance of the inverter between Patch 1 and 2, while J_{23} is the characteristic admittance of the inverter between Patch 2 and 3. k_{12} and k_{23} are the coupling coefficients between the patch radiators.

The ABCD matrix of the circuit between V_1 and V_3 can be obtained by multiplying the ABCD matrix of each element.

$$\begin{bmatrix} A_1 & B_1 \\ C_1 & D_1 \end{bmatrix} = [M_A]\cdot[M_T]\cdot[M_A]\cdot[M_{J1}]\cdot[M_Y]\cdot[M_{J2}] \tag{5}$$

where

$$[M_A] = \begin{bmatrix} 1 & 0 \\ G_A & 1 \end{bmatrix} \quad [M_Y] = \begin{bmatrix} 1 & 0 \\ Y_A & 1 \end{bmatrix} \tag{6a}$$

$$[M_{J1}] = \begin{bmatrix} 0 & -j/J_{12} \\ -jJ_{12} & 0 \end{bmatrix} \quad [M_{J2}] = \begin{bmatrix} 0 & -j/J_{23} \\ -jJ_{23} & 0 \end{bmatrix} \tag{6b}$$

$$[M_T] = \begin{bmatrix} \cos\theta & jZ_{01}\sin\theta \\ j\sin\theta/Z_{01} & \cos\theta \end{bmatrix} \tag{6c}$$

$[M_A]$, $[M_Y]$, and $[M_T]$ are the ABCD matrixes of the parallel radiation conductance, parallel input admittance of patch,

and the transmission line, respectively. $[M_{J1}]$ and $[M_{J2}]$ are the ABCD matrixes of two inverters. According to the definition of ABCD matrix, the relationship between V_1 and V_3 can be obtained.

$$V_1 = A_1 V_3 + B_1 I_3 \tag{7}$$

$$\frac{V_1}{V_3} = A_1 + B_1 \frac{I_3}{V_3} = A_1 + B_1 Y_A = h_1 \sin 2\theta + j(h_2 + h_3 \cos 2\theta) \tag{8}$$

where

$$h_1 = -16\pi \mathrm{Q}\left(\pi^2 + 2\left(8 + \left(k_{12}^2 + k_{23}^2\right)\pi^2\right)Q^2\right) \tag{9a}$$

$$h_2 = -\pi^4 - 4\pi^2\left(-8 + \left(k_{12}^2 + k_{23}^2\right)\pi^2\right)Q^2 - 64\left(4 + \left(k_{12}^2 - k_{23}^2\right)\pi^2\right)Q^4 \tag{9b}$$

$$h_3 = \pi^4 + 4\pi^2\left(24 + \left(k_{12}^2 + k_{23}^2\right)\pi^2\right)Q^2 + 64\left(4 + \left(k_{12}^2 + k_{23}^2\right)\pi^2\right)Q^4 \tag{9c}$$

I_3 is the current that flows into Patch 3 in the equivalent circuit model, as denoted in Fig. 2(c). Similarly, the ABCD matrix of the circuit between V_2 and V_3 is calculated as

$$\begin{bmatrix} A_2 & B_2 \\ C_2 & D_2 \end{bmatrix} = [M_{J2}] \tag{10}$$

Then the relationship between V_2 and V_3 can be obtained as

$$V_2 = A_2 V_3 + B_2 I_3 \tag{11}$$

$$\frac{V_2}{V_3} = A_2 + B_2 \frac{I_3}{V_3} = A_2 + B_2 Y_A = \frac{\left(\pi^2 + 16Q^2\right)\tan\theta - j8\pi Q}{8\pi k_{23} Q^2 + j2\pi^2 k_{23} Q \tan\theta} \tag{12}$$

Thus far, the complex amplitude ratio of the two orthogonal components can be obtained by substituting (8) and (12) into (1). It can be found that the complex amplitude ratio is only determined by the quality factor of the single patch radiator and the coupling coefficients between the adjacent patch radiators. It should be noted that when the patch is at the resonant frequency, the electrical length θ of the patch equals π. Consequently, θ can be transformed to the frequency with the following equation.

$$f/f_0 = \theta/\pi \tag{13}$$

The resonance frequency of the single patch radiator is initially specified in the design. Then the dimension of the single patch radiator is determined for a selected substrate and the quality factor of the single patch radiator can be obtained as well. As a result, there are only two unknown parameters, k_{12} and k_{23}, in the expression of the complex amplitude ratio. Assuming that perfect CP radiation is achieved at the frequency of f_1, the complex amplitude ratio should meet the conditions of equal magnitude and 90° phase difference.

$$V_y/V_x = -j \text{ where } f = f_1 \tag{14}$$

TABLE 1. Parameters in three cases under $Q = 23.5$.

	Case 1	Case 2	Case 3
f_1/f_0	0.981	0.985	0.990
k_{12}	0.08595	0.08596	0.08598
k_{23}	0.0289	0.0250	0.0211

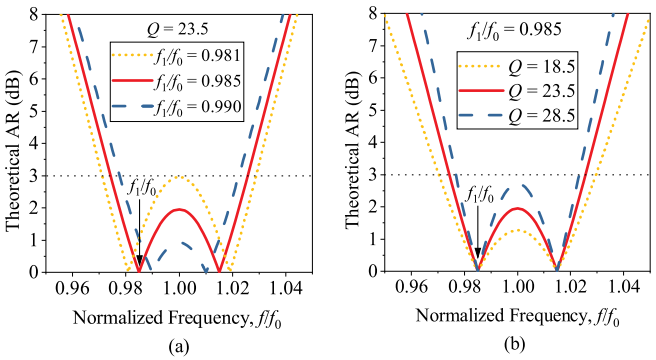

FIGURE 3. Theoretical AR responses under different values of parameters. (a) f_1/f_0. (b) Q.

Two equations are created by expanding the real and imaginary parts of (14), which can be used to calculate two unknown parameters, i.e., k_{12} and k_{23}, can thus be calculated. With all the parameters determined, the AR response can be predicted with the complex amplitude ratio [41, Ch. 2].

$$\gamma = \tan^{-1}\left(V_y/V_x\right), \quad \delta = \varphi\left(V_y/V_x\right) \tag{15a}$$

$$\varepsilon = 0.5\sin^{-1}(\sin(2\gamma)\sin\delta), \quad \mathrm{AR} = \mp 1/\tan(\varepsilon) \tag{15b}$$

where AR and ε are negative in the case of left-hand circular polarization and positive in the case of right-hand circular polarization.

C. THEORETICAL ANALYSIS

The theoretical results obtained using the aforementioned design method are discussed in order to highlight a few attractive features of the proposed CP antenna. Firstly, the AR responses under different frequencies of the AR minimum are investigated. The frequency is normalized with the resonant frequency of the single patch and f_0 is equal to 1. Assuming that the quality factor of the single patch radiator is 23.5. Different values of f_1/f_0 are chosen as shown in Table 1, and the coupling coefficients between coupled radiators can be calculated using the proposed design method. The theoretical AR responses are plotted in Fig. 3(a). It is observed that two minima are generated in the AR response, resulting in a widened bandwidth. Because the frequencies of the two minima are symmetric about the center frequency, only the frequency f_1 is required in the proposed design method. The ripple at the center frequency decreases as two minima in the AR response move inwards. The coupling coefficient k_{12} almost keeps unchanged while k_{23} gradually decreases in these cases. In other words, the frequencies of two minima are mainly affected by the coupling coefficient k_{23} when the quality factor of the single patch is given.

TABLE 2. Parameters in three cases under $f_1/f_0 = 0.985$.

	Case 1	Case 2	Case 3
Q	18.5	23.5	28.5
k_{12}	0.1099	0.08596	0.0706
k_{23}	0.0286	0.0250	0.0231

Secondly, the AR responses under different values of quality factor of the single patch are discussed. The frequency of the minimum in the AR response is set as f_1/f_0=0.985. Different values of Q are chosen as shown in Table 2, and the coupling coefficients between coupled radiators can be calculated with the proposed design method. The theoretical AR responses are plotted in Fig. 3(b). Two minima are observed in the AR response and their positions of minima remain unchanged as expected. When the quality factor of the single patch increases, the ripple at the center frequency rises, and the 3-dB bandwidth decreases. The required coupling coefficient k_{12} decreases significantly while k_{23} changes only slightly. As a result, the coupling coefficient k_{12} is primarily determined by the quality factor of the patch radiator.

Thirdly, the 3-dB AR bandwidth of the proposed CP antenna is investigated. As shown in Fig. 3(a), for a given Q, the ripple at the center frequency will reach 3 dB by moving two minima in the AR response. In this case, the theoretical maximum 3-dB AR bandwidth is obtained for the given Q. The AR bandwidth of the proposed CP antenna is compared with the one of the traditional CP patch antenna. As discussed in [41], the AR bandwidth of the traditional CP patch antenna based on two degenerate modes can be calculated as follows.

$$BW_{CP}^{AR} \approx 0.115 \frac{AR_{\max}^{dB}}{Q} \tag{16}$$

where ARmax dB is the maximum allowable axial ratio in [dB].

The 3-dB AR bandwidths of the proposed and traditional CP patch antennas under different values of Q are shown in Fig. 4. When Q increases from 16 to 30, the fractional bandwidth (FBW) of the proposed antenna is reduced from 8.4% to 4.5%, while the FBW of the traditional CP patch antenna decreases from 2.2% to 1.2%. It can be found that the FBW of the proposed antenna is almost 3.5 times that of the traditional CP patch antenna. Furthermore, the required coupling coefficients can be calculated using the proposed design method at the same time, as shown in Fig. 4. When Q increases from 16 to 30, the coupling coefficient, k_{12} and k_{23}, gradually decrease from 0.13 to 0.07 and from 0.043 to 0.023, respectively. It can be found that k_{12} is always larger than k_{23}. From the point-view of physical insight, the values of coupling coefficients determine the ratio of power divided to each patch. The configuration of k_{12} and k_{23} in our design ensures that the two orthogonal far-field components can satisfy the magnitude condition for CP radiation.

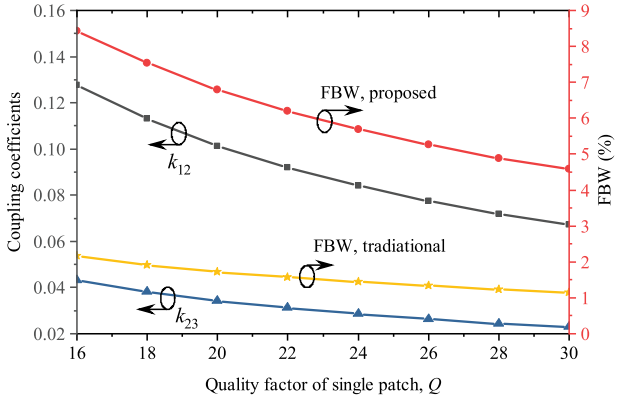

FIGURE 4. Coupling coefficients and fractional bandwidth (FBW) under different values of Q.

TABLE 3. Dimensional parameters of the proposed antenna in Fig. 1.

Parameters	p	g_1	g_2	W_{p1}	L_{p1}	W_{p2}	L_{p2}	W_{p3}	L_{p3}
Value (mm)	7.0	0.3	2.4	12	26.5	12	27.4	12	27.0

D. SIMULATION AND EXPERIMENTAL VERIFICATION

Next, the proposed antenna structure and design method are verified by full-wave simulation and experiment. The whole antenna structure is implemented on a single-layer substrate with a thickness of 3 mm, relative permittivity of 2.2, and loss tangent of 0.0012. The resonant frequency is set to 3.48 GHz and then the length of each patch can be determined when the width of the patch is set to 12 mm. Then the quality factor of a single patch can be extracted by full-wave simulation, which is 23.5 in this design. The frequency of the AR minimum is chosen as $f_1/f_0 = 0.985$. The required coupling coefficients can be calculated with the proposed design method, which are $k_{12} = 0.086$ and $k_{23} = 0.025$. As seen from the geometry of the proposed antenna in Fig. 1, it can be understood that k_{12} and k_{23} vary as a function of the coupling gaps (g_1 and g_2). The values of coupling coefficient (k) under specified physical dimensions can be numerically extracted by two natural resonant frequencies (f_{01} and f_{02}) of two coupled patch radiators via full-wave simulation [43].

Thus, the initial physical dimensions can be determined. After minor fine tuning, the final physical dimensions can all be determined as tabulated in Table 3. It should be noted that the lengths of the three patch radiators are slightly changed due to the effects of coupling and the feeding probe.

As shown in Fig. 5, the simulated magnitude ratio (MR) and phase difference (PD) of two orthogonal far-field components are compared with the theoretical ones, which agree well with each other. In the operating band, small ripples around 1 and $-90°$ appear in the magnitude ratio and phase difference responses, respectively. Two minima appear in the magnitude ratio response. The phase difference response is almost antisymmetric around the center frequency. One peak is slightly larger than $-90°$ below the center frequency and

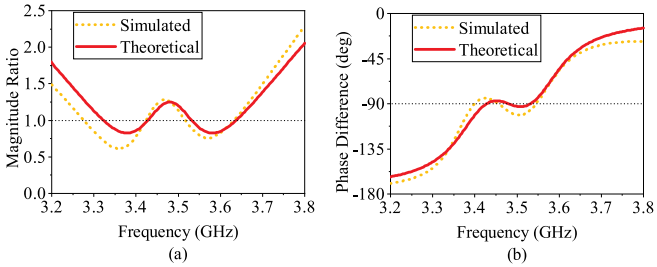

FIGURE 5. Comparison between the theoretical and simulated results of the proposed CP antenna with 3 coupled patch radiators. (a) Magnitude ratio. (b) Phase difference.

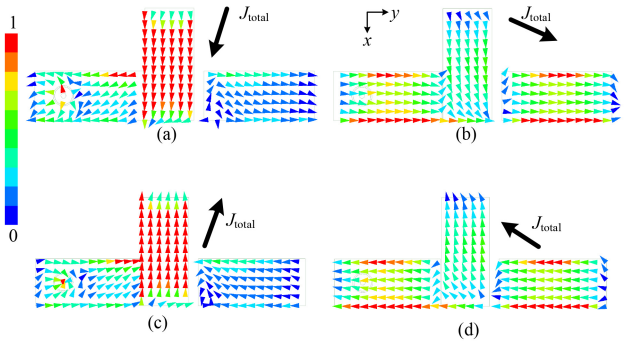

FIGURE 6. Simulated surface current distributions of the proposed CP antenna with 3 coupled patches at 3.425 GHz over a single period. (a) $t = 0$. (b) $t = 1/4T$. (c) $t = 2/4T$. (d) $t = 3/4T$.

one minimum is slightly smaller than $-90°$ above the center frequency. Fig. 6 plots the simulated surface current distributions of the proposed CP antenna with 3 coupled patches at 3.425 GHz over a single period. At $t = 0$, the surface currents on Patch 1, 2, and 3 are along $-y$, $+x$, and $+y$ axis directions, respectively. The currents on Patch 1 are stronger than those on Patch 3. Thus, the total equivalent surface current is along the lower left direction. Similarly, at $t = 1/4T$, $2/4T$, and $3/4T$, the total equivalent surface current directions are indicated in Fig. 7(b), (c), and (d), respectively. During one period, the current direction rotates anticlockwise, producing right-handed circularly polarized radiation wave.

Fig. 7 shows the simulated $|S_{11}|$ and AR responses of the proposed CP antenna with 3 coupled patches under different values of gaps. When g_{12} increases, the magnitude and the center frequency of the reflection coefficient decrease, resulting in better impedance matching. When g_{12} increases from 0.2 to 0.3 and 0.4 mm, the frequency of the left minimum in the AR response decreases from 3.435 to 3.426 and 3.416 GHz while the right one remains nearly unchanged. The resulting AR bandwidth is extended as the ripple in the center frequency rises. When g_{23} changes from 2.2 to 2.4 and 2.6 mm, both the two minima in the AR response move inwards, resulting in decreased bandwidth and ripple variation.

Next, the proposed CP antenna is fabricated and measured for further verification. The antenna is measured

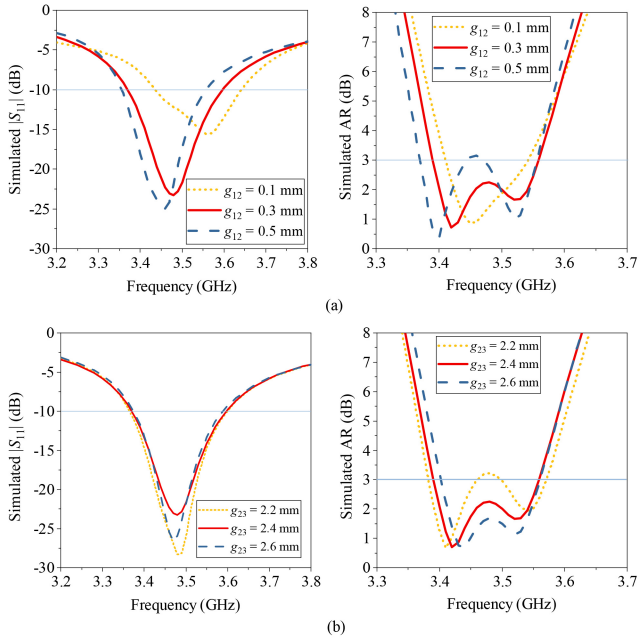

FIGURE 7. Simulated $|S_{11}|$ and AR responses of the proposed CP antenna with 3 coupled patches under different values of gaps. (a) g_{12}. (b) g_{23}.

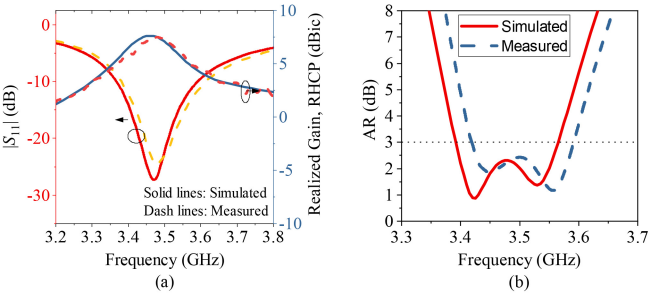

FIGURE 8. Simulated and measured reflection coefficients, realized gains, and AR responses of the proposed CP antenna with 3 coupled patch radiators.

using Keysight E5071C Vector Network Analyzer (VNA) for reflection coefficients and SUNYIELD SY-16M antenna measurement system for radiation characteristics, respectively. The simulated and measured results of reflection coefficients, realized gains and AR responses are plotted in Fig. 8. The results show good agreement between the simulated and measured values, except for a small frequency shift. The measured 10-dB return-loss bandwidth is from 3.38 to 3.61 GHz, with only one minimum in the reflection coefficient response. It should be noted that the couplings between patch radiators affect the performances of AR and S_{11} at the same time. In our design, the coupling coefficients are specified to obtain multiple minima in the AR response. However, under these coupling coefficients between patch radiators, the response of S_{11} may not be optimal, and multiple reflection zeros can not be achieved at the same time. Despite this, the 10-dB return-loss bandwidth is still sufficient. The peak realized gain is 7.56 dBic, and the realized gain response sharply rolls down outside the operating

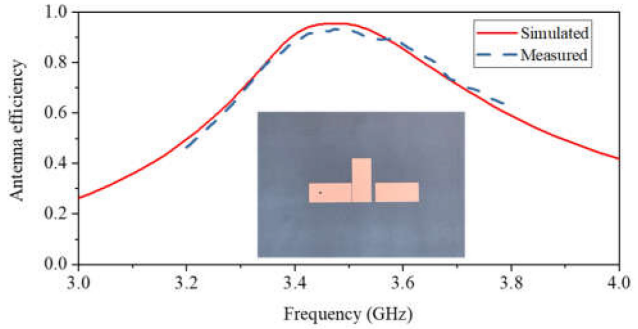

FIGURE 9. Simulated and measured efficiencies of the proposed CP antenna with 3 coupled patch radiators.

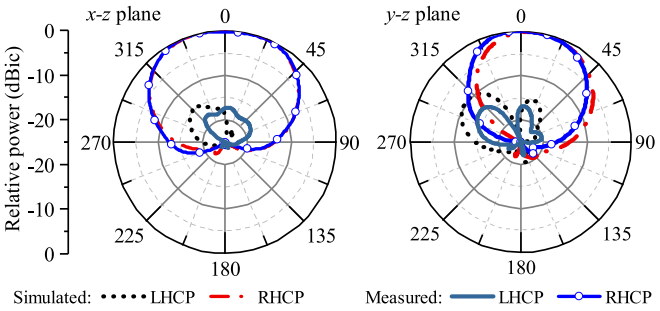

FIGURE 10. Simulated and measured normalized LHCP and RHCP radiation patterns of the proposed CP antenna with 3 coupled patch radiators at 3.5 GHz.

band. The measured 3-dB gain bandwidth is from 3.35 to 3.59 GHz. The simulated AR response matches well with the measured one, except for a small frequency discrepancy. It is found that the frequency shift of S_{11} is slightly smaller than that of AR. This is because the AR response is more sensitive to the antenna configuration, and the discrepancy may be caused by the assembly error of the feeding part and tolerance of the antenna dimension. Two minima come up at around 3.45 GHz and 3.55 GHz, which efficiently broadens the AR bandwidth. The fractional bandwidth with AR<3 dB is 4.7% and 4.9% in the simulation and measurement, respectively. The measured 3-dB AR bandwidth ranges from 3.42 to 3.59 GHz. Consequently, the overlap bandwidth of reflection coefficient, realized gain, and AR is from 3.42 to 3.59 GHz and the corresponding fractional bandwidth is 4.9%.

The simulated and measured efficiencies agree well with each other, as shown in Fig. 9. The efficiency in the operating band is approximately 90%. The normalized left-hand circularly polarized (LHCP) and right-hand circularly polarized (RHCP) far-field radiation patterns in both x-z and y-z planes are measured at 3.5 GHz and the results are presented in Fig. 10. The simulated radiation patterns agree well with the measured ones, and boresight radiation is obtained as expected. The RHCP field intensity is approximately 17 dB higher than that of the LCHP counterpart in the boresight direction. The measured half-power

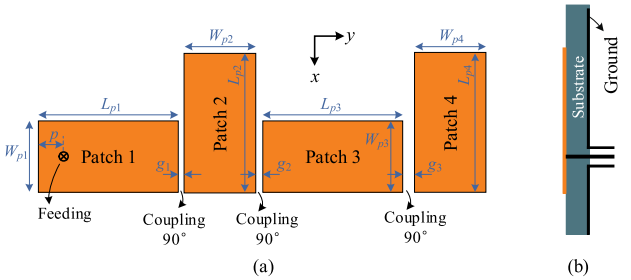

FIGURE 11. The geometry of the proposed CP antenna with 4 coupled radiators. (a) Top view. (b) Side view.

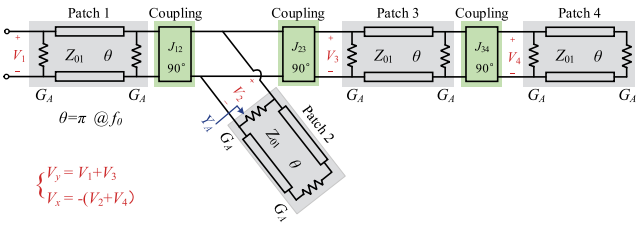

FIGURE 12. Equivalent circuit model of the proposed CP antenna with 4 coupled radiators in Fig. 11.

beamwidths in the x-z and y-z planes are found to be 94.5° and 63.5°, respectively. These two values are different because the geometry of the proposed antenna is not symmetrical.

III. CP ANTENNA WITH FOUR COUPLED RADIATORS

A. GEOMETRY AND DESIGN

In this section, the radiator number of the proposed CP antenna is increased to 4 to achieve wider bandwidth, and the antenna's geometry is depicted in Fig. 11. Similarly, 4 patch radiators are placed one by one along x- and y-axes, and each patch radiators are in proximity to the next one. TM_{01} modes are excited in Patches 1 and 3, and TM_{10} modes are excited in Patches 2 and 4. The corresponding equivalent circuit model is shown in Fig. 12, which is similar to the one of the CP antenna with three coupled patch radiators. The patch antenna can be equivalent as a half-wavelength transmission line with two parallel radiation conductances at two ends, and the coupling between the patch radiators is modeled as a J inverter. The voltages (V_x and V_y) of the patch resonators in the equivalent circuit model correspond to the radiation fields [17], [34], [35]. Therefore, the complex amplitude ratio of the two orthogonal far-field components is given by

$$\frac{V_y}{V_x} = \frac{V_1 + V_3}{-(V_2 + V_4)} = \frac{V_1/V_4 + V_3/V_4}{-(V_2/V_4 + 1)} \tag{17}$$

where V_1, V_2, V_3, and V_4 are the excitation voltage of Patches 1, 2, 3, and 4, respectively.

Following that, V_1, V_2, and V_3 are tried to be expressed with V_4, which can be calculated with the ABCD matrix as discussed in the previous section. It can be derived that the complex amplitude ratio in (17) is only determined by

TABLE 4. Parameters in three cases for the antenna in Fig. 11.

	Case 1	Case 2	Case 3
f_1/f_0	0.96	0.97	0.98
k_{12}	0.13178	0.13183	0.13187
k_{23}	0.05985	0.04895	0.04058
k_{34}	0.03070	0.02479	0.01924

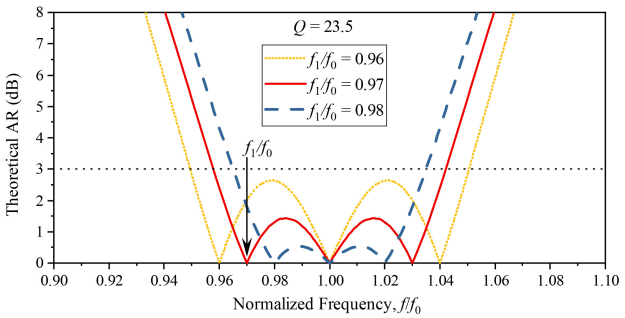

FIGURE 13. Theoretical AR responses of the proposed antenna with 4 coupled radiators under different values of f_1/f_0.

TABLE 5. Dimensional parameters of the proposed antenna in Fig. 11.

Parameters	p	g_1	g_2	g_3	W_{p1}	L_{p1}	W_{p2}	L_{p2}
Value (mm)	7.5	0.2	1.9	2.1	12	26.0	12	27.5
Parameters	W_{p3}	L_{p3}	W_{p4}	L_{p4}				
Value (mm)	12	26.7	12	27.2				

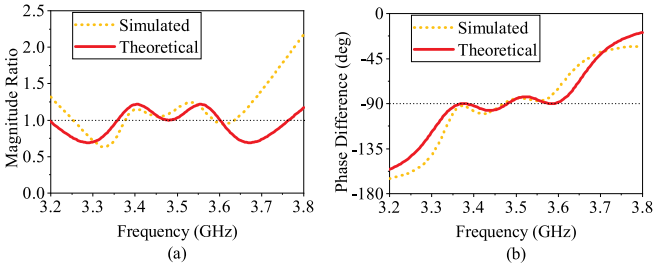

FIGURE 14. Comparison between the theoretical and simulated results of the proposed CP antenna with 4 coupled patch radiators. (a) Magnitude ratio. (b) Phase difference.

the quality factor of the single patch (Q) and the coupling coefficients (k_{12}, k_{23}, and k_{34}). k_{34} is related to the inverter J_{34}, which is expressed as

$$k_{34} = \frac{J_{34}}{b_r} = \frac{2J_{34}}{\pi Y_{01}} \tag{18}$$

In the design, the quality factor of the single patch is given at first. Assuming that perfect CP radiation is achieved at the frequency of f_0 and f_1, the complex amplitude ratio should meet the conditions of equal magnitude and 90° phase difference.

$$V_y/V_x = -j \text{ where } f = f_0 \tag{19a}$$
$$V_y/V_x = -j \text{ where } f = f_1 \tag{19b}$$

It should be noted that the complex amplitude ratio is a pure imaginary quantity at f_0. So only one equation is obtained from (19a). However, by expanding the real and imaginary parts of (19a) and (19b), three equations are obtained with three unknown parameters, and so k_{12}, k_{23}, and k_{34}, can be calculated.

Assuming that the quality factor of the single patch is 23.5, different values of f_1/f_0 are chosen, as shown in Table 4. The required coupling coefficients can be calculated with the proposed design method, and AR responses are also obtained, as plotted in Fig. 13. Three minima appear in the AR response to form a wide bandwidth. As two minima outside the center frequency move inwards, the in-band ripples gradually decline and the minimum in the center frequency remains unchanged. As a result, the AR bandwidth gradually decreases. As shown in Table 4, the coupling coefficient k_{12} is almost kept unchanged, while k_{23} and k_{34} gradually decrease. Therefore, for a given Q, the AR minima are mainly determined by k_{23} and k_{34}.

B. SIMULATION AND EXPERIMENTAL VERIFICATION

The proposed CP antenna in this section is also implemented on a single-layer substrate with a thickness of 3 mm, relative permittivity of 2.2, and loss tangent of 0.0012. The resonant frequency and width of the single patch are set as 3.48 GHz and 12 mm, respectively. The extracted quality factor of the single patch is 23.5. The frequency of the AR minimum is given by $f_1/f_0 = 0.97$. The required coupling coefficients can be calculated with the proposed design method, which are figured out with $k_{12} = 0.1318$, $k_{23} = 0.048$, and $k_{34} = 0.025$. k_{12}, k_{23}, and k_{34} will vary with the coupling gap widths g_1, g_2, and g_3, respectively. The initial physical dimensions can be determined by numerical extraction of coupling coefficients in full-wave simulation. After minor fine tuning, the final physical parameters are determined and tabulated in Table 5.

In Fig. 14, the simulated magnitude ratio, phase difference, and AR responses of the antenna are compared with the theoretical ones. The simulated results match well with the theoretical ones, verifying the proposed design method. Small ripples of the magnitude ratio and phase difference responses appear in the operating band. One more ripple appears in both the magnitude ratio and phase difference responses when compared to the responses of the CP antenna with three coupled patch radiators in Fig. 5. In the theoretical magnitude ratio response, the values of the local minimum at the center frequency reaches 1. In the theoretical response of phase difference, the local maximum at low frequency and the local minimum at high frequency are both exactly −90°.

The simulated surface current distributions of the proposed CP antenna with 4 coupled patches at 3.465 GHz over a single period are plotted in Fig. 15. The surface currents on Patch 1 and 3 are along $-y$ axis direction, while those on Patch 2 and 4 are along $+x$ axis direction, as shown in Fig. 15(a). The total equivalent current is along the lower

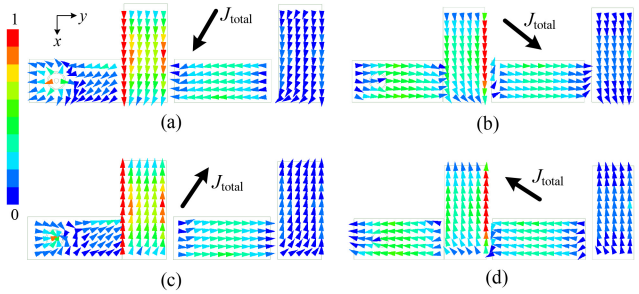

FIGURE 15. Simulated surface current distributions of the proposed CP antenna with 4 coupled patches at 3.465 GHz over a single period. (a) $t = 0$. (b) $t = 1/4T$. (c) $t = 2/4T$. (d) $t = 3/4T$.

left direction. Similarly, it can be found that the total equivalent surface current direction rotates anticlockwise during one period as shown in Fig. 15. The simulated $|S_{11}|$ and AR responses of the proposed CP antenna with 4 coupled patches under different values of gaps are plotted in Fig. 16. As g_{12} increases, both the magnitude and frequency of the minimum of the reflection coefficient decrease. When g_{12} increases from 0.1 to 0.2 and 0.3 mm, the ripples of the AR response increase and the two left minima move towards low frequency. When g_{23} increases from 1.5 to 1.9 and 2.3 mm, the center frequency of reflection coefficient nearly remains unchanged, but the magnitude increases. The value of g_{23} mainly affects the frequency of the right minimum in the AR response. When g_{23} increases, the right minimum moves towards low frequency. There is little effect of g_{34} on the $|S_{11}|$ response. The variation of g_{34} mainly affects the symmetrical property of the AR response. As g_{34} increases, the left ripple goes down while the right one rises.

The proposed CP antenna with 4 coupled patch radiators is fabricated and measured. Fig. 17 depicts the simulated and measured reflection coefficients, realized gains, and AR responses. Good agreement is observed between simulation and measurement. The measured 10-dB return-loss bandwidth is from 3.36 to 3.69 GHz. The peak realized gain is 7.75 dBic and the measured 3-dB realized gain bandwidth covers the frequency range of 3.34 to 3.60 GHz. There is a small frequency discrepancy between the simulated and measured AR responses, with the center frequency shifting from 3.48 to 3.50 GHz. Three minima appear in the AR response to construct enhanced bandwidth. The simulated and measured fractional bandwidths with AR<3 dB are 7.3% and 7.1%, respectively. The measured 3-dB AR bandwidth ranges from 3.38 to 3.63 GHz. As a result, the overlap bandwidth of reflection coefficient, realized gain, and AR is from 3.38 to 3.60 GHz, and the corresponding fractional bandwidth is 6.3%.

The simulated and measured efficiencies in Fig. 18 match well with each other, although the measured efficiency is slightly lower than the simulated one. Specifically, the simulated and measured efficiencies at 3.48 GHz are 93% and 88.6%, respectively. Fig. 19 shows the simulated and measured results of normalized radiation patterns at 3.5 GHz

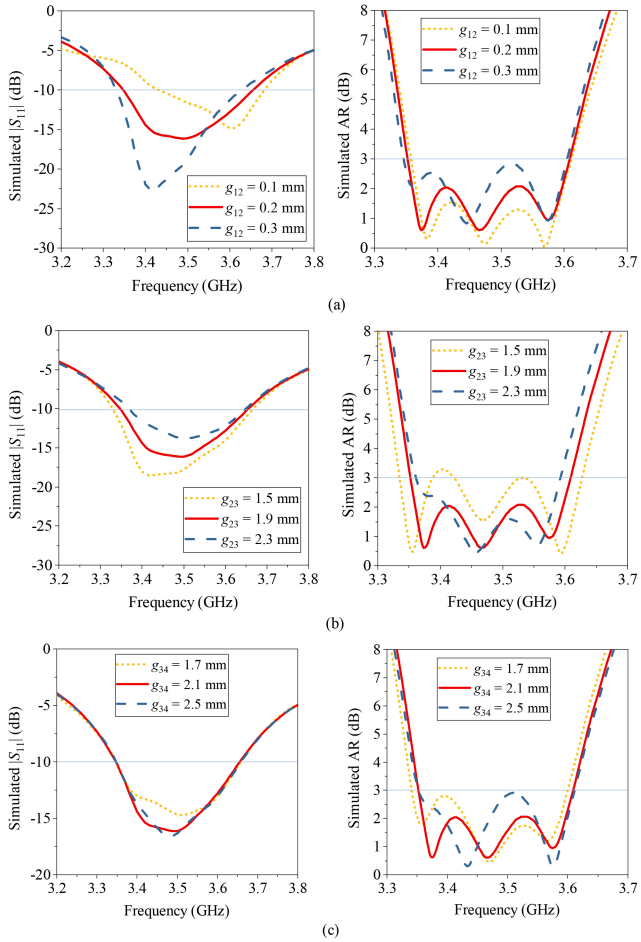

FIGURE 16. Simulated $|S_{11}|$ and AR responses of the proposed CP antenna with 4 coupled patches under different values of gaps. (a) g_{12}. (b) g_{23}. (c) g_{34}.

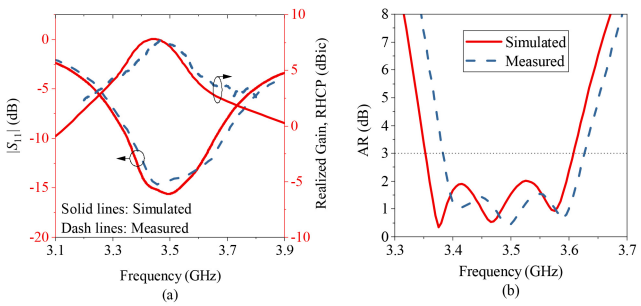

FIGURE 17. Simulated and measured reflection coefficients, realized gains, and AR responses of the proposed CP antenna with 4 coupled patch radiators.

and good agreement is observed. The measured half-power beamwidth in the x-z and y-z planes are 96° and 58.5°, respectively. The maximum cross-polarization levels in the x-z and y-z planes are −17.6 dB and −15.7 dB, respectively. Therefore, the proposed CP antenna can radiate satisfactory RHCP waves with low cross-polarization.

IV. CP ANTENNA WITH MORE COUPLED RADIATORS

In the previous two sections, wideband CP antennas with three and four coupled radiators are designed, and two and

TABLE 6. Property comparison among different wideband CP patch antennas.

Ref.	Structure	Feed Type	Total Size (λ_0^3)	Overlap Bandwidth (%)	Peak Gain (dBic)	Extra Feeding Circuit	Approaches
[11]	multi-layer	multi-feed	0.59*0.59*0.15	16	~8	yes	sequential feed, parasitic element
[12]	multi-layer	single feed	0.63*0.63*0.13	24	~8	no	parasitic elements
[13]	single layer	single feed	0.92 *0.92 *0.028	12.9	9.8	no	parasitic elements
[14]	single layer	single feed	0.50*0.27*0.016	3	2.7	no	parasitic elements
[15]	single layer	single feed	0.51*0.52*0.03	5	~4.5	no	multi-mode
[18]	single layer	single feed	0.55*0.23*0.114	25.4	7.4	no	E-shape patch
[20]	single layer	single feed	1.04*1.04*0.027	14.3	8.9	no	parasitic elements
[25]	multi-layer	multi-feed	~1.8*1.8*0.12	62	8.1	yes	wideband phase shifter
[26]	multi-layer	multi-feed	0.78*0.71*0.12	61.7	~6.5	yes	wideband phase shifter
[27]	multi-layer	multi-feed	1.13*1.13*0.15	96.3	9.5	yes	sequential feed, phase shifter
[28]	multi-layer	multi-feed	0.87*0.87*0.05	47.8	9.05	yes	wideband phase shifter
[34]	multi-layer	multi-feed	0.53*0.53*0.07	12.2	~5.2	yes	filtering circuit
[36]	multi-layer	multi-feed	0.92*0.92*0.04	6.2	7	yes	filtering circuit
This Work	single layer	single feed	0.32*0.95*0.035	6.3	7.75	no	orthogonal coupled patches

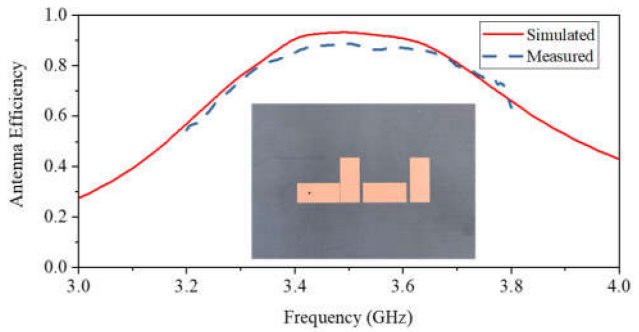

FIGURE 18. Simulated and measured efficiencies of the proposed CP antenna with 4 coupled patch radiators.

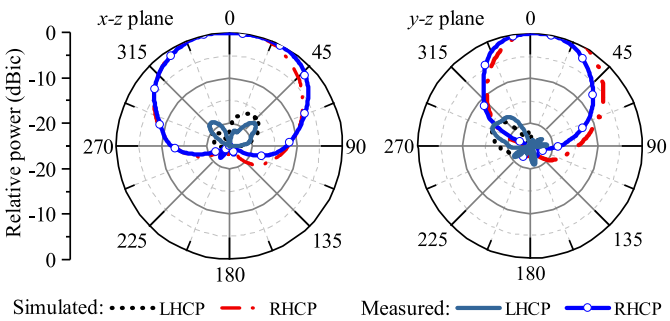

FIGURE 19. Simulated and measured normalized LHCP and RHCP radiation patterns of the proposed CP antenna with 4 coupled patch radiators at 3.5 GHz.

three minima in the AR response are achieved. Similarly, the CP antenna with more coupled orthogonal patch radiators can be further designed. Multiple patch radiators are placed one by one along the *x*- and *y*-axes and the adjacent patch radiators are coupled to each other. Then the proposed design method can be employed to calculate the required coupling coefficients between adjacent coupled radiators and predict the AR response. In theory, for the CP antenna with n coupled radiators, $n - 1$ minima in the AR response can be produced to form a wide bandwidth. If more than 4 coupled radiators are employed, wider bandwidth is achieved but a larger coupling coefficient is required. The theoretical procedure of the proposed design method may become more complicated. To address this, the multiple patches can be placed on the multiple layers to obtain strong coupling and more compact size. Furthermore, based on the same design method, the patch radiators can be replaced with other kinds of antenna radiators, such as slot antenna.

After that, a comprehensive comparison among different wideband CP patch antennas is summarized in Table 6. The size of the proposed antenna is $0.32*0.95\lambda_0^2$ and the profile is $0.035\lambda_0$. Our work exhibits medium size and low profile, when compared to other wideband CP patch antennas. It can be seen that the works in [11], [12], [25], [26], [27], [28], [34], and [36] employ multi-layer structures or sequentially rotated patches, suffering from complex configuration. Extra feeding circuits consisting of Wilkinson power divider and wideband phase shifter are utilized, which occupy large area. The unbalanced signals are absorbed by the resistor of the power divider to ensure equal magnitude and quadrature phase for wide AR bandwidth. But the antenna efficiency will be degraded. Among the single-layer structures [13], [14], [15], [16], our work exhibits medium bandwidth and gain under a low profile. In [13] and [14], parasitic elements are employed but no synthesis design method is reported. The antenna design mainly replies on time-consuming full-wave simulation. The thick substrate is used in [18], resulting in the high profile and increased cost. Finally and importantly, if compared with these reported works, a clear design mechanism and a quantitative design method based on the equivalent circuit model are proposed in this paper. Multiple coupled patches are employed to introduce multiple minima

in the AR response to form wide bandwidth. The coupled patches serve as both radiators and feeding networks at the same time. There is no need for an additional feeding circuit in the design, resulting in a compact structure. The required coupling coefficients can be calculated to determine the physical dimensions. The magnitude ratio and phase difference of the orthogonal far-field components, as well as the AR response, can be accurately predicted, improving design efficiency significantly.

V. CONCLUSION

CP patch antennas with enhanced bandwidth based on capacitively coupled orthogonal patch radiators have been proposed in this paper. A quantitative design method based on the equivalent circuit model and closed-form solution has been proposed to efficiently design and analyze the proposed antenna. Wideband CP patch antennas with three and four coupled radiators are designed, fabricated, and measured. Multiple minima appear in the AR response to form wide bandwidth. The theoretical and full-wave simulation results are found to be in good agreement. The proposed antenna and design method are furtherly verified by the measurement. The wideband CP radiation characteristic and simple structure make the proposed antenna a good candidate for a variety of applications. Furthermore, the proposed antenna can be employed as a subarray element to construct a large-scale antenna array with enhanced radiation gain.

REFERENCES

[1] R. Shaw and M. K. Mandal, "Broadside scanning fixed frequency LWA with simultaneous electronic control of beam angle and beamwidth," *IEEE Trans. Antennas Propag.*, vol. 68, no. 5, pp. 3504–3514, May 2020.

[2] Y. Zhang et al., "A broadband high-gain circularly polarized wide beam scanning leaky-wave antenna," *IEEE Access*, vol. 8, pp. 171091–171099, 2020.

[3] S. Ge, Q. Zhang, A. K. Rashid, Y. Zhang, H. Wang, and R. Murch, "A compact full-space scanning leaky-wave antenna with stable peak gain," *IEEE Trans. Antennas Propag.*, vol. 69, no. 10, pp. 6924–6929, Oct. 2021.

[4] F.-S. Chang, K.-L. Wong, and T.-W. Chiou, "Low-cost broadband circularly polarized patch antenna," *IEEE Trans. Antennas Propag.*, vol. 51, no. 10, pp. 3006–3009, Oct. 2003.

[5] K.-F. Tong and T.-P. Wong, "Circularly polarized U-slot antenna," *IEEE Trans. Antenna Propag.*, vol. 55, no. 8, pp. 2382–2385, Aug. 2007.

[6] A. Khidre, K. F. Lee, F. Yang, and A. Elsherbeni, "Wideband circularly polarized E-shaped patch antenna for wireless applications," *IEEE Antennas Propag. Mag.*, vol. 52, no. 5, pp. 219–229, Oct. 2010.

[7] S. S. Yang, K.-F. Lee, A. A. Kishk, and K.-M. Luk, "Design and study of wideband single feed circularly polarized microstrip antennas," *Progr. Electromagn. Res.*, vol. 80, pp. 45–61, Jan. 2008.

[8] J. M. Kovitz and Y. Rahmat-Samii, "Using thick substrates and capacitive probe compensation to enhance the bandwidth of traditional CP patch antennas," *IEEE Trans. Antennas Propag.*, vol. 62, no. 10, pp. 4970–4979, Oct. 2014.

[9] Q. W. Lin, H. Wong, X. Y. Zhang, and H. W. Lai, "Printed meandering probe-fed circularly polarized patch antenna with wide bandwidth," *IEEE Antennas Wireless Propag. Lett.*, vol. 13, pp. 654–657, 2014.

[10] W.-W. Yang, W.-J. Sun, W. Qin, J.-X. Chen, and J.-Y. Zhou, "Broadband circularly polarised stacked patch antenna with integrated dual-feeding network," *IET Microw. Antennas Propag.*, vol. 11, no. 12, pp. 1791–1795, Sep. 2017.

[11] S. Fu, Q. Kong, S. Fang, and Z. Wang, "Broadband circularly polarized microstrip antenna with coplanar parasitic ring slot patch for L-band satellite system application," *IEEE Antennas Wireless Propag. Lett.*, vol. 13, pp. 943–946, 2014.

[12] J. Wu, Y. Yin, Z. Wang, and R. Lian, "Broadband circularly polarized patch antenna with parasitic strips," *IEEE Antennas Wireless Propag. Lett.*, vol. 14, pp. 559–562, 2015.

[13] K. Ding, C. Gao, D. Qu, and Q. Yin, "Compact broadband circularly polarized antenna with parasitic patches," *IEEE Trans. Antennas Propag.*, vol. 65, no. 9, pp. 4854–4857, Sep. 2017.

[14] J.-F. Lin and Q.-X. Chu, "Enhancing bandwidth of CP microstrip antenna by using parasitic patches in annular sector shapes to control electric field components," *IEEE Antennas Wireless Propag. Lett.*, vol. 17, pp. 924–927, 2018.

[15] N.-W. Liu, L. Zhu, Z.-X. Liu, G. Fu, and Y. Liu, "Design approach of a single circularly polarized patch antenna with enhanced AR-bandwidth under triple-mode resonance," *IEEE Trans. Antennas Propag.*, vol. 68, no. 8, pp. 5827–5834, Aug. 2020.

[16] N. Nasimuddin, Z. N. Chen, and X. Qing, "Bandwidth enhancement of a single-feed circularly polarized antenna using a metasurface: Metamaterial-based wideband CP rectangular microstrip antenna," *IEEE Antennas Propag. Mag.*, vol. 58, no. 2, pp. 39–46, Apr. 2016.

[17] G. Kumar and K. Gupta, "Broad-band microstrip antennas using additional resonators gap-coupled to the radiating edges," *IEEE Trans. Antennas Propag.*, vol. 32, no. 12, pp. 1375–1379, Dec. 1984.

[18] J. Zeng, X. Liang, L. He, F. Guan, F. H. Lin, and J. Zi, "Single-fed triple-mode wideband circularly polarized microstrip antennas using characteristic mode analysis," *IEEE Trans. Antennas Propag.*, vol. 70, no. 2, pp. 846–855, Feb. 2022.

[19] X. Zhang et al., "Analysis and design of stable-performance circularly-polarized antennas based on coupled radiators for smart watches," *IEEE Trans. Antennas Propag.*, vol. 70, no. 7, pp. 5312–5323, Jul. 2022.

[20] Z. Chen et al., "Enhancing circular polarization performance of low-profile patch antennas for wearables using characteristic mode analysis," *Sensors*, vol. 23, no. 5, p. 2474, Feb. 2023.

[21] W. Zhou et al., "Impact of amplitude and phase imbalance on dual differential fed patch antenna with high isolation," *IEEE Open J. Antennas Propag.*, vol. 3, pp. 1227–1233, 2022.

[22] X. M. Qing, "Broadband aperture-coupled circularly polarized microstrip antenna fed by a three-stub hybrid coupler," *Microw. Opt. Technol. Lett.*, vol. 40, no. 1, pp. 38–41, Nov. 2004.

[23] M. Haneishi and Y. Suzuki, "Circular polarization and bandwidth," in *Handbook of Microstrip Antennas*. London, U.K.: Peregrinus, 1989, pp. 220–273.

[24] L. Bian, Y.-X. Guo, L. C. Ong, and X.-Q. Shi, "Wideband circularly-polarized patch antenna," *IEEE Trans. Antenna Propag.*, vol. 54, no. 9, pp. 2682–2686, Sep. 2006.

[25] Y.-X. Guo, K.-W. Khoo, and L. C. Ong, "Wideband circularly polarized patch antenna using broadband baluns," *IEEE Trans. Antenna Propag.*, vol. 56, no. 2, pp. 319–326, Feb. 2008.

[26] J. Zhuang, Y. Zhang, W. Hong, and Z. Hao, "A broadband circularly polarized patch antenna with improved axial ratio," *IEEE Antennas Wireless Propag. Lett.*, vol. 14, pp. 1180–1183, 2015.

[27] Q. Liu, Z. N. Chen, Y. Liu, and C. Li, "Compact ultrawideband circularly polarized weakly coupled patch array antenna," *IEEE Trans. Antennas Propag.*, vol. 65, no. 4, pp. 2129–2134, Apr. 2017.

[28] L.-L. Qiu, L. Zhu, and Y. Xu, "Wideband low-profile circularly polarized patch antenna using 90° modified Schiffman phase shifter and meandering microstrip feed," *IEEE Trans. Antennas Propag.*, vol. 68, no. 7, pp. 5680–5685, Jul. 2020.

[29] K. L. Chung, "High-performance circularly polarized antenna array using metamaterial-line based feed network," *IEEE Trans. Antennas Propag.*, vol. 61, no. 12, pp. 6233–6237, Dec. 2013.

[30] M. Salarrahimi, V. Volski, and G. A. E. Vandenbosch, "Mutual coupling-based compact wideband circularly polarized antenna," *IEEE Trans. Antennas Propag.*, vol. 67, no. 7, pp. 4872–4877, Jul. 2019.

[31] C.-X. Mao et al., "An integrated filtering antenna array with high selectivity and harmonics suppression," *IEEE Trans. Microw. Theory Techn.*, vol. 64, no. 6, pp. 1798–1805, Jun. 2016.

[32] K.-R. Xiang, F.-C. Chen, Q. Tan, and Q.-X. Chu, "High-selectivity filtering patch antennas based on multipath coupling structures," *IEEE Trans. Microw. Theory Techn.*, vol. 69, no. 4, pp. 2201–2210, Apr. 2021.

[33] T. Li and X. Gong, "Vertical integration of high-*Q* filter with circularly polarized patch antenna with enhanced impedance-axial ratio bandwidth," *IEEE Trans. Microw. Theory Techn.*, vol. 66, no. 6, pp. 3119–3128, Jun. 2018.
[34] Z. H. Jiang and D. H. Werner, "A compact, wideband circularly polarized co-designed filtering antenna and its application for wearable devices with low SAR," *IEEE Trans. Antennas Propag.*, vol. 63, no. 9, pp. 3808–3818, Sep. 2015.
[35] Y. Lu, Y. Wang, S. Gao, C. Hua, and T. Liu, "Circularly polarised integrated filtering antenna with polarisation reconfigurability," *IET Microw. Antennas Propag.*, vol. 11, no. 15, pp. 2247–2252, Dec. 2017.
[36] Q.-S. Wu, X. Zhang, and L. Zhu, "A wideband circularly polarized patch antenna with enhanced axial ratio bandwidth via co-design of feeding network," *IEEE Trans. Antennas Propag.*, vol. 66, no. 10, pp. 4996–5003, Oct. 2018.
[37] C.-X. Mao, S. Gao, Y. Wang, Q.-X. Chu, and X.-X. Yang, "Dual-band circularly polarized shared-aperture array for *C*-/ *X*-band satellite communications," *IEEE Trans. Antennas Propag.*, vol. 65, no. 10, pp. 5171–5178, Oct. 2017.
[38] C.-X. Mao, S. S. Gao, Y. Wang, and J. T. S. Sumantyo, "Compact broadband dual-sense circularly polarized microstrip antenna/array with enhanced isolation," *IEEE Trans. Antennas Propag.*, vol. 65, no. 12, pp. 7073–7082, Dec. 2017.
[39] M.-C. Tang, D. Li, Y. Wang, K.-Z. Hu, and R. W. Ziolkowski, "Compact, low-profile, linearly and circularly polarized filtennas enabled with custom-designed feed-probe structures," *IEEE Trans. Antennas Propag.*, vol. 68, no. 7, pp. 5247–5256, Jul. 2020.
[40] M. Haneishi and S. Yoshida, "A design method of circularly polarized rectangular microstrip antenna by one-point feed," *Electron. Commun. Jpn. I, Commun.*, vol. 64, no. 4, pp. 46–54, Apr. 1981.
[41] W. L. Langston and D. R. Jackson, "Impedance, axial-ratio, and receive-power bandwidths of microstrip antennas," *IEEE Trans. Antennas Propag.*, vol. 52, no. 10, pp. 2769–2773, Oct. 2004.
[42] J. D. Kraus and R. J. Marhefka, *Antennas for All Applications*, 3rd ed. New York, NY, USA: McGraw-Hill, 2001.
[43] J.-S. Hong and M. J. Lancaster, *Microstrip Filters for RF/Microwave Applications*. New York, NY, USA: Wiley, 2001.

QIONG-SEN WU received the B.Eng. degree in information engineering and the M.Eng. degree in electromagnetism and microwave engineering from the South China University of Technology, Guangzhou, China, in 2011 and 2014, respectively, and the Ph.D. degree in electrical and computer engineering from the University of Macau, Macau, SAR, China, in 2018.

He joined the Guangdong University of Technology, China, as a Lecture in June 2018, and became an Associate Professor in 2022. His current research interests include microwave circuits and planar antennas with improved functionalities. He also serves as a Reviewer for several journals, including the IEEE TRANSACTIONS ON ANTENNAS AND PROPAGATION and the IEEE TRANSACTIONS ON MICROWAVE THEORY AND TECHNIQUES.

XIAO-YU TANG, photograph and biography not available at the time of publication.

XIAO ZHANG (Member, IEEE) was born in Gaozhou, Guangdong, China. He received the B.Eng. degree in information engineering and the M.Eng. degree in communication and information systems from the South China University of Technology, Guangzhou, China, in 2011 and 2014, respectively, and the Ph.D. degree in electrical and computer engineering from University of Macau, Macau, SAR, China, in 2017.

He was a Research Assistant with Comba Telecom Systems Limited, Guangzhou, from September 2012 to August 2014 and a Research Fellow with the Antenna and Electromagnetic-Wave Laboratory, University of Macau from January 2018 to March 2018. He is currently an Assistant Professor with the College of Electronics and Information Engineering, Shenzhen University, Shenzhen, China. He was recognized as the Shenzhen Overseas High Caliber Personnel Level C in 2018. He was recognized as the Top 2% Scientists in 2019 by Elsevier. His research interests include high-gain antennas, wideband antennas, circularly-polarized antennas, terminal antennas, filtering antennas, reflectarray, and characteristic mode analysis.

Dr. Zhang was the recipient of the Scientific and Technological Research and Development Award for Postgraduates of Macau in 2018. He also serves as a Reviewer for several journals, including the IEEE TRANSACTIONS ON ANTENNAS AND PROPAGATION and the IEEE ANTENNAS AND WIRELESS PROPAGATION LETTERS.

LEI ZHU (Fellow, IEEE) received the B.Eng. and M.Eng. degrees in radio engineering from the Nanjing Institute of Technology (currently Southeast University), Nanjing, China, in 1985 and 1988, respectively, and the Ph.D. degree in electronic engineering from The University of Electro-Communications, Tokyo, Japan, in 1993.

He was a Research Engineer with Matsushita-Kotobuki Electronics Industries Ltd., Tokyo, Japan, from 1993 to 1996, a Research Fellow with the École Polytechnique de Montréal, Montreal, QC, Canada, from 1996 to 2000, and an Associate Professor with the School of Electrical and Electronic Engineering, Nanyang Technological University, Singapore, from 2000 to 2013. He joined the Faculty of Science and Technology, University of Macau, Macau, China, as a Full Professor in August 2013, and has been a Distinguished Professor since December 2016. From August 2014 to August 2017, he served as the Head of Department of Electrical and Computer Engineering, University of Macau. So far, he has authored or coauthored more than 750 papers in international journals and conference proceedings. His papers have been cited more than 15 000 times with the H-index of 61 (source: Scopus). His research interests include microwave circuits, antennas, periodic structures, and computational electromagnetics.

Dr. Zhu was the recipient of the 1997 Asia–Pacific Microwave Prize Award, the 1996 Silver Award of Excellent Invention from Matsushita-Kotobuki Electronics Industries Ltd., the 1993 Achievement Award in Science and Technology (First Prize) from the National Education Committee of China, the 2020 FST Research Excellence Award from the University of Macau, and the 2020 and 2022 Macao Natural Science Awards (Second Prize) from the Science and Technology Development Fund (FDCT), Macau. He was an Associate Editor for the IEEE TRANSACTIONS ON MICROWAVE THEORY AND TECHNIQUES from 2010 to 2013 and IEEE MICROWAVE AND WIRELESS COMPONENTS LETTERS from 2006 to 2012. He served as the General Chair of the 2008 IEEE MTT-S International Microwave Workshop Series on the Art of Miniaturizing RF and Microwave Passive Components, Chengdu, China, the Technical Program Committee Co-Chair of the 2009 Asia–Pacific Microwave Conference, Singapore, a member of IEEE MTT-S Fellow Evaluation Committee from 2013 to 2015, and a member of IEEE AP-S Fellow Committee from 2015 to 2017.

GARY ZHANG, photograph and biography not available at the time of publication.

CHUN-BING GUO, photograph and biography not available at the time of publication.